at −60 °C and filtered. The solid product remaining on the frit, compound Id, turned green, and the soluble fraction was proven to contain KBH_4 upon analysis.

Acknowledgment. Analyses were done by the Analytical Chemistry Division of the Oak Ridge National Laboratory. I wish to thank J. H. Burns for a valuable discussion.

Registry No. $TiBr_4$, 7789-68-6; KBH_4, 13762-51-1; NH_3, 7664-41-7; $TiCl_3$, 7705-07-9; $NaBH_4$, 16940-66-2.

Contribution from the Department of Chemistry and Institute of Materials Science and Department of Chemical Engineering, University of Connecticut, Storrs, Connecticut 06268

Chromium(III)-Doped Pillared Clays (PILC's)

K. A. Carrado,[†] S. L. Suib,*[†] N. D. Skoularikis,[‡] and R. W. Coughlin*[‡]

Received March 21, 1986

Spectroscopic and catalytic properties of a low-iron-content bentonite clay were found to be sensitive to pillaring and to exchange with Cr(III) ions. These ions were introduced into the clay in both pillared and unpillared forms by the use of different synthetic conditions. Diffuse reflectance spectroscopy (DRS) and electron paramagnetic resonance (EPR) were used to monitor the environment of Cr(III) to determine whether it was in the interlamellar space of the clay or associated with an aluminum–hydroxy pillar. Catalytic behavior responded differently to Cr(III) in the different environments. Incorporating Cr(III) into an alumina pillar increased the kinetic stability and activity of the catalyst in decane cracking compared to a PILC catalyst containing no chromium.

I. Introduction

It is known that smectite clays can be pillared with oligomeric metal hydroxide ions[1-3] to yield thermally stable materials with some properties similar to those of zeolites. Moreover, these materials have pores of a larger size range that allows catalytic conversion of high molecular weight hydrocarbons.[2]

Pillared montmorillonites have been prepared by ion exchanging the clay with several different agents, some of which are hydroxy–aluminum[4] cations $\{[Al_{13}O_4(OH)_{24}(H_2O)_{12}]^{7+}\}$, zirconyl–aluminum–halo–hydroxy complexes[4] $\{[ZrOCl_2{\cdot}Al_8(OH)_{20}]^{4+}\}$, colloidal silica,[4] polyoxy–chromium oligomers,[5] and zirconyl chloride[6] $\{[Zr_4(OH)_{16-n}(H_2O)_{n+8}]^{n+}\}$ and fluoro–hydroxy–aluminum cations[7] $\{[Al_{13}O_4F_x(OH)_{24-x}]^{7+}\}$.

These materials display different catalytic activities depending upon the type of pillar and upon the presence of other metallic ions or complexes. Propylene oligomerization has been examined with alumina-pillared clays (APC) and (Zr,Al)PC.[8] The catalytic cracking activity of APC has been extensively studied.[2,9,10] Increased acidity and related catalytic activity have been examined by pillaring preexchanged Ce– and La–clays.[11,12] By also adding other metal or metal complex ions to a pillared clay, other catalytic mechanisms have been induced; APC (Zr,Al)PC, and clays pillared with silica have been evaluated for use as the cracking component for hydrocracking vacuum gas oil.[4] Fischer–Tropsch (F–T) catalytic properties of metal cluster carbonyl complexes on APC[13] and the re-forming activity of Pt–Re on APC[14] have also been reported. Pillaring of a nickel-substituted montmorillonite produces hydroisomerization catalysts.[15] Also, $Ru(NH_3)_6^{3+}$-exchanged APC has been observed[16] to have activity for the reduction of CO_2 by H_2.

Here we report observed differences in the catalytic role played by a supported metal ion depending upon its apparent position in a pillared clay, i.e. in the micropore structure vs. in the pillars. Related work has attempted to substitute uranyl[17] and iron[18] ions directly into an alumina or zirconia pillar. Chromium ions were chosen because they can be tracked spectroscopically, as has been reported for Cr^{3+}-exchanged zeolites by using infrared spectroscopy, electron paramagnetic resonance (EPR), and diffuse reflectance spectroscopy (DRS).[19] The photochemical and photocatalytic properties of tris(2,2′-bypyridine)chromium(III) in clays[20] have also been studied. Hydroxy–chromium cations in clays have been examined.[21,22] The catalytic activity of chromium as chromia, Cr_2O_3, has been reported in reactions[23] involving alkylation, aromatization, cracking, cyclization, dehydrogenation, F–T, hydrodealkylation, hydrogenation, oxidation, re-forming, and the water gas shift reaction. Chromia-pillared clay catalysts have recently been studied for the dehydrogenation of cyclohexane to benzene.[5]

A relevant study has recently disclosed a class of hydroprocessing catalysts reported[24] to be comprised of, for example, a Ni^{2+} or Co^{2+} ion-exchanged smectite that is then cross-linked with hydroxy–Al oligomers. This material is calcined at 400–500 °C and treated with, for example, an ammonium molybdate solution to yield the hydroprocessing catalyst.

* To whom correspondence should be addressed.
[†] Department of Chemistry and Institute of Materials Science.
[‡] Department of Chemical Engineering.

(1) Vaughan, D. E. W.; Lussier, R. J. *Proc. Int. Conf. Zeol., 5th* **1980**, 94.
(2) Vaughan, D. E. W.; Lussier, R. J.; Magee, J. S. U.S. Patent 4 176 090, 1979.
(3) Lahav, N.; Shani, U.; Shabtai, J. *Clays Clay Miner.* **1978**, *26*, 107.
(4) Occelli, M. L.; Rennard, R. J., submitted for publication.
(5) Pinnavaia, T. J.; Tzou, M. S.; Landau, S. D. *J. Am. Chem. Soc.* **1985**, *107*, 4783.
(6) Yamanaka, S.; Brindley, G. W. *Clays Clay Miner.* **1979**, *27*, 119.
(7) Fijal, J.; Shabtai, J. *Abstracts of Papers*, International Clay Conference, Denver, CO, 1985; No. 67.
(8) Occelli, M. L.; Hsu, J. T.; Galya, L. G. *J. Mol. Catal.* **1985**, *33*, 371.
(9) Occelli, M. L.; Innes, R. A.; Hwu, F. S. S.; Hightower, J. W. *Appl. Catal.* **1985**, *14*, 69.
(10) Occelli, M. L. *Ind. Eng. Chem. Prod. Res. Dev.* **1983**, *22*, 553.
(11) Tokarz, M.; Shabtai, J. *Clays Clay Miner.* **1985**, *33*, 89.
(12) Shabtai, J.; Lazar, R.; Oblad, A. G. *Proceeding of the 7th Inter. Congress on Catalysis*; Seiyama, T., Tanabe, K., Eds.; Kodansha-Elsevier: Tokyo, 1980; p 828.
(13) Giannelis, E. P.; Rightor, E. G.; Pinnavaia, T. J. *Abstracts of Papers*, International Clay Conference, Denver, CO, 1985; No. 81.
(14) Parulekar, V. N.; Hightower, J. W. *Abstracts of Papers*, 9th Meeting of the Catalysis Society, Houston, TX, 1985.
(15) Gaaf, J.; van Santen, R.; Knoester, A.; van Wingerden, B. *J. Chem. Soc., Chem. Commun.* **1983**, 655.
(16) Challal, D.; Bergaya, F.; van Damme, H. *Bull. Soc. Chim. Fr.* **1985**, *3*, 393.
(17) Occelli, M. L.; Tanguay, J. F.; Suib, S. L. *J. Am. Chem. Soc.*, in press.
(18) Kostapapas, A.; Suib, S. L.; Skoularikis, N. D.; Coughlin, R. W., submitted for publication.
(19) Pearce, J. R.; Sherwood, D. E.; Hall, M. B.; Lunsford, J. H. *J. Phys. Chem.* **1980**, *84*, 3215.
(20) Krenske, D.; Abdo, S.; van Damme, H.; Cruz, M.; Fripiat, J. J. *J. Phys. Chem.* **1980**, *84*, 2447. Abdo, S.; Canesson, P.; Cruz, M.; Fripiat, J. J.; van Damme, H., *J. Phys. Chem.* **1981**, *85*, 797.
(21) Brindley, G. W.; Yamanaka, S. *Am. Mineral.* **1979**, *64*, 830.
(22) Carr, M. *Clays Clay Miner.* **1985**, *33*, 357.
(23) Wagner, F. S. In *Applied Industrial Catalysis*; Leach, B. E., Ed.; Academic: New York, 1983, Vol. 2, p 39.
(24) Shabtai, J.; Fijal, J. U.S. Patent 4 579 832, 1986.

0020-1669/86/1325-4217$01.50/0

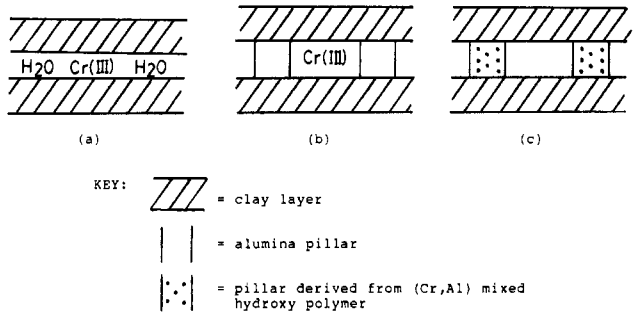

Figure 1. Schematic representation of clays and pillared clays indicating presumed location of Cr(III) ions: (a) Cr–b (b) Cr–pb (c) Cr*–pb.

Three different synthetic routes were employed, seeking to incorporate chromium ions in different locations in the clays as schematically shown in Figure 1. Spectroscopic evidence for the existence of these different types of structures was obtained by DRS and EPR; basal spacings were determined with X-ray powder diffraction (XRD) methods. Clay catalysts prepared by the three different procedures and spectroscopically characterized were also investigated as to differences in catalytic activity for cracking *n*-decane.

II. Experimental Section

A. Sample Preparation. Materials. Bentolite L (a bentonite clay referred to as b) was used as received in its Ca^{2+}-exchanged form from Southern Clay Products, TX. This clay is reported to be composed of 71.7% SiO_2, 15.7% Al_2O_3, 3.6% MgO, 1.7% CaO, 0.3% Fe_2O_3 and TiO_2, 0.2% Na_2O, and 0.16% K_2O. The cation-exchange capacity was quoted by the supplier as 80 mequiv/100 g and the particle size as less than 1.0 μm. The purity of *n*-decane (Aldrich Co.) as measured by GC was 99.97%.

Sample Cr–b. Ion exchange of Bentolite L (b) by Cr(III) ions was carried out by slurrying clays (1 wt %) in various concentrations of $Cr(H_2O)_6^{3+}$ derived from $CrCl_3 \cdot 6H_2O$ (Aldrich Chem. Co.). This product is represented in Figure 1a.

Sample pb. Pillared clays (pb = pillared bentonite) were prepared by using a procedure described by Occelli and co-workers.[25] To a slurry of 1 wt % clay in distilled, deionized water (DDW) was added 1 mL/(g of clay) of an aluminum–hydroxy polymer solution marketed by Reheis Chemical Co. under the tradename of Chlorhydrol (ACH). The pillaring cation in this solution[25] is believed to be $[Al_{13}O_4(OH)_{24}(H_2O)_{12}]^{7+}$.

Sample Cr–pb. A sample containing Cr(III) ions in the micropore structure of a pillared clay was prepared by pillaring Cr–b, the Cr-(III)-exchanged bentonite. Figure 1c shows the product presumed to arise from this method; here Cr(III) is not directly associated with the pillar.

Sample Cr*–pb. The asterisk indicates that Cr(III) ions are in the pillars of the clay; the pillaring aluminum–hydroxy cation was doped with Cr(III) ions, as represented by Figure 1b, by a procedure used to incorporate UO_2^{2+} ions.[17]

The details of pillaring with ACH and the mixed-ion polymer solutions are given elsewhere, along with conditions for hydrations and heat treatments.[26]

B. Spectroscopy. The crystallinity of the materials was studied by X-ray powder diffraction using a DIANO-XRD 8000 X-ray powder diffractometer equipped with a Philips Electronic source. Basal spacings were determined either by a small-angle X-ray camera or via powder techniques using a Norelco instrument also equipped with a Philips Electronic source. Spectra were calibrated with a standard silicon powder disk.

Ultraviolet–visible spectroscopy of solutions was studied with a Perkin-Elmer Lambda 3B UV/vis spectrophotometer. Diffuse reflectance spectra (DRS) of solids were recorded on the same instrument using an integrating sphere attachment (250–850 nm). Clays as loose powders were placed in 2-mm quartz spectroscopy cells. $BaSO_4$ was used as a reference material.

Electron paramagnetic resonance spectra of the clays were measured on either an E-3 or E-9 Varian X-band spectrometer at room temperature. The *g* values are calculated relative to a 2,2′-diphenyl-1-picrylhydrazyl (DPPH) standard. Samples were sealed off in quartz tubes evacuated to at least 1×10^{-3} Torr.

Thermal gravimetric analyses (TGA) were obtained with a Cahn 113X instrument using a heating rate of 10 °C/min in static air.

Determination of wt % chromium for each sample was done by atomic absorption spectroscopy; samples were dissolved in dilute hydrofluoric acid.

The products of clay-catalyzed reactions were assigned and identified by a Hewlett-Packard Model 5985B GC/MS. The same columns were also used for routine temperature-programmed chromatographic analyses.

C. Decane Cracking. Catalysts (1.5g as a powder or pellets) were placed in a heated (400 °C) stainless-steel tubular reactor and pretreated with hydrogen (31.6 mL/min) for 90 min. A syringe pump then injected *n*-decane into the H_2 feed stream at a flow rate of 0.07 mL/min. After 15 s the gaseous products (2 mL) were diverted to a GC column using a sampling valve. One reaction cycle consisted of injection of *n*-decane as above for a period of 40 s followed by hydrogen treatment of the catalyst for 30 min. At least eight such cycles were performed for each catalyst. The sampling valve (Carle 22115) was held at 230 °C, and the GC column was 10 wt % Carbowax 20M on 80/100 mesh Supelcoport from Supelco, Inc. Helium was used as a carrier gas (40 mL/min). Satisfactory separation of the reaction products was achieved by temperature programming from 130 to 220 °C at a rate of 10 °C/min. A flame-ionization detector was used (hydrogen, 42.5 mL/min; air, 140 mL/min).

Blank experiments (reactor charged with glass beads only) were performed under the same conditions. The extent of thermal cracking with glass beads was on the order of 1%.

Table I. Chromium Content of Clay Samples

sample	wt %
Cr–b	1.37
Cr–pb	1.22
Cr*–pb	0.44

Table II. X-ray Diffraction, Diffuse Reflectance, and Thermal Gravimetric Data of Cr-Containing Clays

sample	d_{001}, Å: before catalysis[a]	d_{001}, Å: after catalysis[a]	DRS, nm	wt % H_2O[b]
Cr–b	14.3	*c*	415, 589	16.9
pb	19.0	18.0	UV	22.1
Cr*–pb	18.4	17.80	415 sh, 587	20.1
Cr–pb	18.4	broad (~17)	406, 581	15.7
Cr(III)/ACH crystals			416, 588	
$Cr(H_2O)_6^{3+}$			408, 576	

[a] 400 °C/H_2/1 h pretreatment; cycles of *n*-decane. [b] wt % H_2O lost over 20–720 °C range via TGA. [c] Peak not apparent, indicating delamination.

III. Results

A. Characterization. Clays were analyzed for chromium content by atomic absorption spectroscopy, and the results are given in Table I.

Table II lists basal spacings for the d_{001} reflection of each material both before and after exposure to decane as catalysts for cracking reactions. Values between 14 and 15 Å were common for unpillared clays, while pillared clays showed spacings from 17 to 19 Å. Thermal analysis experiments were done to monitor the wt % water lost from each sample on heating; the values are recorded in Table II.

Also shown in Table II are the wavelengths of the absorbance maxima in diffuse reflectance spectra of each of the samples. Reflectance data for crystals of an evaporated 0.1 M Cr(III) solution in ACH are also recorded here. Samples b and pb exhibited absorbance in the UV region only (400 nm and lower). Hence, all other clay materials also displayed this band in the DRS experiments.

Figure 2 shows the relative DRS absorbances in the Cr(III) region for the chromium-containing clays and for the green crystals of Cr(III)/ACH.

Diffuse reflectance data for various hydration and calcination experiments of Cr–clays are reported in Table III and presented in Figure 3. Chromium(III) transitions were observed after the

(25) Occelli, M. L.; Tindwa, R. M. *Clays Clay Miner.* **1983**, *31*, 22.
(26) Carrado, K. A. Ph.D. Thesis, University of Connecticut, Storrs, CT, 1986.

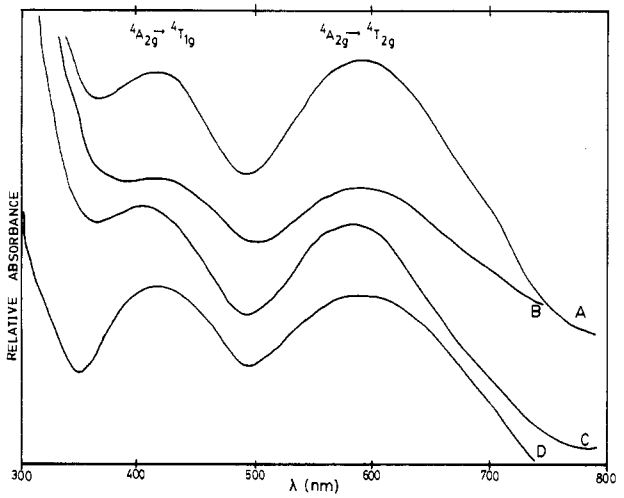

Figure 2. Diffuse reflectance spectra of (A) Cr–b, (B) Cr*–pb, (C) Cr–pb, and (D) Cr(III)–ACH crystals.

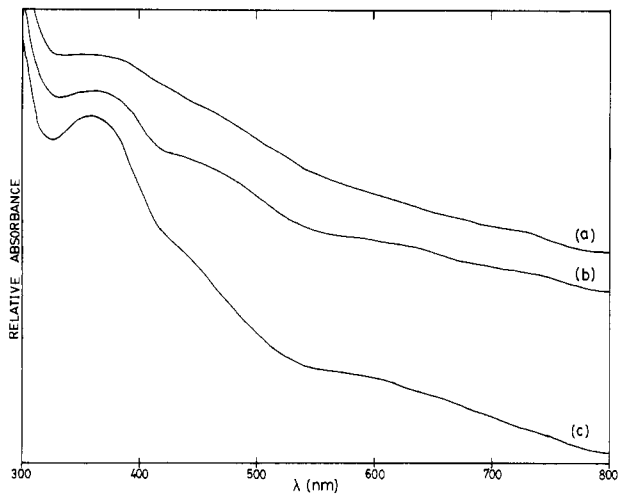

Figure 3. Diffuse reflectance spectra of (a) calcined Cr–b (300 °C/5 h/air), (b) calcined Cr–b exposed to 100% H_2O vapor for 24 h, and (c) calcined Cr–pb exposed to 100% H_2O vapor for 18 h.

Table III. Diffuse Reflectance Spectra (nm) for Hydration and Calcination of Cr-Containing Clays[a]

sample	air-dried	hydrated[b]	calcined[c]	rehydrated[d]
Cr–b	415, 589	416, 586	360 wk	360, 440 sh, 580 w, 720 w
Cr*–pb	415 sh, 587	415 sh, 585	350 wk, 600 sh	360, 450 sh, 580 sh
Cr–pb	406, 581	405, 579	360 sh, 580 sh	365, 440 sh, 580 sh

[a] Samples subsequently air-dried, hydrated, calcined, then rehydrated. Key: w = weak, sh = shoulder. [b] Placed in 100% humidity for 18–24 h. [c] Heated at 300 °C for 5 h in air.

samples were air-dried, hydrated, calcined in air, and then rehydrated to monitor the behavior of the ion under various conditions of oxidation and hydration.

EPR data for Cr–clays, both before and after oxidation, are given in Table IV. A range in g values was observed from 1.918 to 2.076 as well as a wide range in peak widths from 25 to 1000 G. Figure 4 shows the EPR signals for selected samples both before and after oxidation.

B. Cracking Experiments. Conversion is plotted vs. the number of cycles in Figure 5 for each catalyst. The heavy products of the reaction were identified via GC/MS using temperature-programmed GC analysis, and their yields were calculated. Identified products included pentane, hexane, 3-ethyl-1-pentene, cyclooctane, benzene, ethylbenzene, xylenes, and poly-substituted aromatics. The major intermediate products were usually hexane isomers with

Table IV. EPR Data for Cr-Containing Clays[a]

sample no.	g value	H_{pp}, G	assignment
Cr–b	1.974	400	Cr(III)
Cr–b calcined[b]	none		Cr(III), Cr(VI)
Cr*–pb	2.051	312	Cr(III)
Cr*–pb calcined[b]	1.961	50	Cr(V)
	bkgd	br	Cr(III)
Cr–pb	2.072	668	Cr(III)
Cr–pb calcined[b]	2.076	1080	Cr(III)
	1.970	c	Cr(V) $g_\perp$
	1.944	<25	Cr(V) $g_\parallel$
	1.918	<25	Cr(V) $g_\parallel$

[a] Room temperature; corrected to DPPH. [b] 300 °C/5 h/air. [c] Not determined.

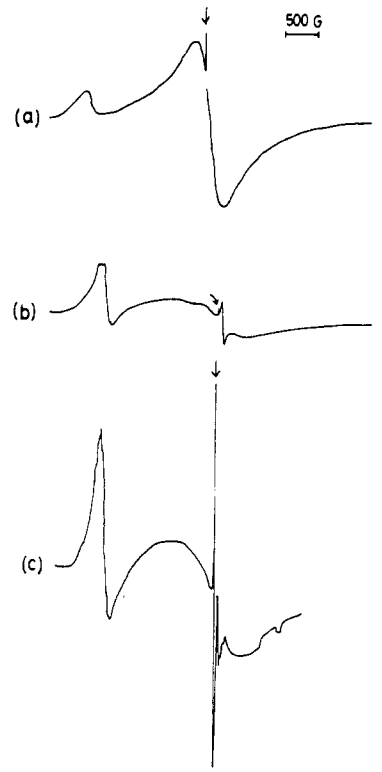

Figure 4. EPR spectra taken at 25 °C for (a) Cr–b, (b) Cr*–pb treated at 300 °C/5 h/air, and (c) Cr–pb treated at 300 °C/5 h/air. The arrow in each case indicates DPPH. Power, 2–3.5mW; time constant, 0.3–1.0 s; 2–5 G modulation amplitude; 8×10^3 to 1.25×10^5 gain. The signal at $g = 4.1997$ is due to iron in the clay.

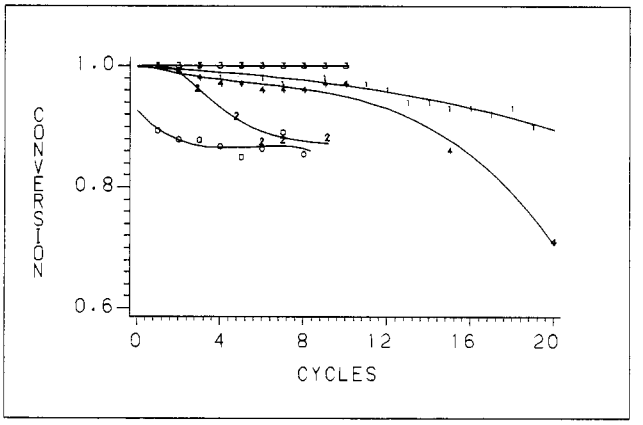

Figure 5. Conversion of *n*-decane in cracking experiments for Cr–clay catalysts and bentonite. The numbers indicating data points correspond to the followng samples: 0, b; 1, Cr–b; 3, Cr*–pb; 4, Cr–pb.

yields ranging from 0% to 45%.

Table V summarizes product yields averaged over the total number of cycles. The extent of coking was determined gravi-

Table V. Yields[a] (wt %) from Decane Cracking

sample	cycles	light gases	hexane[b]	C_7–C_{10} olef & paraf	C_8–C_{21} aromatics	coke[c]
b	8	31	46	0.17	0.63	22
Cr–b	37	64	31	0.08	0.80	4
pb	9	54	6.9	0.12	0.69	38
Cr*–pb	10	78	0.012	0.003	0.044	22
Cr–pb	25	42	26	0.10	0.84	12

[a] Average values over all cycles. [b] Total hexane isomers. [c] Yield of coke as a fraction of hydrocarbon feed; computed from the mass of coke measured gravimetrically after the indicated number of cycles.

metrically via TGA. The yields of light gases were obtained by difference; the presence of C_1–C_5 hydrocarbons was confirmed by GC using a Porapak Q column (Alltech Assoc.).

IV. Discussion

A. Spectroscopic Characterization of Clays. 1. Structural Studies. Table I gives chromium contents for the various samples. For zeolite work[19], low Cr(III)-exchange levels were selected (1.2 wt %) because earlier reports indicated that higher concentrations result in zeolite lattice decomposition. Cr–b shows 1.37 wt % Cr; subsequent pillaring to form Cr–pb decreases the amount only slightly, to 1.22 wt %, indicating that most of the Cr(III) ions are not exchanged by the aluminum–hydroxy cation. As expected, a lower Cr content of 0.44 wt % is observed for Cr*–pb; association with the aluminum–hydroxy pillaring cation does not incorporate as much Cr in the clay as simple ion exchange.

The basal spacings measured by XRD are given in Table II; they are as expected for unpillared and pillared clays, with d_{001} approximately 14 and 18–19 Å, respectively. Heating pillared clays (500 °C/air) results in a decrease in the d_{001} spacing of about 0.5 Å, and this is thought to be due to the formation of alumina pillars.[1]

2. Reflectance Data. Evidence for the location of Cr(III) ions in these different materials is provided by the DRS data in Table II. The spectra are shown in Figure 2. Clays b and pb without chromium(III) present display only a large absorbance from 400 nm through the UV region. This is assigned to charge-transfer bands with a shoulder of much lower intensity near 370 nm that may be indicative of traces of iron present in the clay lattice. $Fe(H_2O)_6^{3+}$ is reported[27] to have a transition at 409 nm. Bentolite H, a clay with a higher concentration of iron, displayed a more intense band in this region. A similar experiment done for zeolite Na–Y, a material with virtually no iron present, did not display any absorbance in this region.

Observed transitions corresponding to Cr(III) appear to be similar whether the ions are in the interlamellar space (Cr–b) or presumed associated with the pillar (Cr*–pb). This could be due to the similar aluminum oxide environment present around chromium(III) in both materials. An indication that Cr(III) is associated with the pillaring ion is seen by comparing the spectrum of Cr*–pb with that of the precipitate formed by evaporating a 0.1 M Cr^{3+} solution in ACH (Cr(III)/ACH). These transitions occur at roughly the same wavelength, within 1 nm. The shoulder (sh) near 415 nm for Cr*–pb may arise from association of Cr(III) with the pillar in the clay, since this behavior is not observed for the other materials.

Sample Cr–pb, in which it is presumed that Cr(III) is not associated with the pillar, displays a unique spectrum. The transitions in this material occur at a significantly higher energy with a blue shift of 7–10 nm. This may arise from the presence of Cr(III) in a more solution-like environment in this material; in other words, more water ligands may be present in the coordination sphere. The bands[27] for the exchange cation $Cr(H_2O)^{3+}$ occur at 408 and 576 nm.

Thermogravimetric data for the catalysts are also given in Table II. Over a temperature range of 700 °C a constant decrease in weight was observed and assigned to the gradual loss of water from the surface and then from the micropore structure of the bentonite. Previous workers[25] have reported an inflection point at 500 °C and attributed it to the loss of hydroxyl water associated in part with the ACH pillars; we did not observe such an inflection point. Less water (15–17%) is lost from Cr–b and Cr–pb than from both pb and Cr*–pb (20–22%), as shown in Table II. This may be an indication that a significant amount of water is present in the micropores of these latter materials.

A final indication that Cr(III) is in the pillar of Cr*–pb is given by the basal spacings after catalytic cracking experiments. Both pb and Cr*–pb remain pillared, while both Cr–b and Cr–pb display less order. The d_{001} reflection for the latter groups of materials either disappears or becomes very broad, indicating that delamination has taken place to at least some extent. The persistence of other reflections indicates all materials remain crystalline after cracking experiments.

Results from various hydration/dehydration experiments are given in Table III. For all materials listed, hydration does not produce marked changes in the diffuse reflectance spectra; only a slight shift of the $^4A_{2g} \rightarrow {}^4T_{2g}$ transition of chromium(III) occurs. Upon oxidation at 300 °C for 5 h in air, a new band near 360 nm appears simultaneously with the loss of the 405–415 and 580–590 nm bands. We believe that the broad background and the band near 360 nm, which are evident in the spectra of Figure 3, may be attributed to Cr(III), but in an environment of lowered symmetry. This is consistent with data obtained for Cr(III)-exchanged zeolites.[19] Oxidation of the clays followed by rehydration is not fully reversible under these conditions; the bands near 440 and 580 nm reappear only to a small degree. The band near 360 nm also becomes more apparent on rehydration. This band may indicate the presence of yet another species; it was not assigned in related work with zeolites.[19]

3. EPR Experiments. Freshly prepared samples display a broad, isotropic EPR signal with $g \sim 2.0$ and a width of several hundred gauss, as shown in Figure 4a. Similar spectra have been reported for Cr(III)-exchanged zeolites[19] and attributed to hexaaquochromium(III). Oxidized samples (300 °C/5 h/air) produced different EPR results as seen in Table IV and Figure 4. No EPR signal was observed for oxidized Cr–b and this may be due to an extreme broadening of the Cr(III) EPR signal caused by reduced symmetry. This is again in line with zeolite work.[19] In addition, any Cr(III) converted to diamagnetic Cr(VI) would no longer contribute to the EPR spectrum. This interpretation is in accord with the DRS data for the same sample in which Cr(III) of low symmetry was observed. Oxidation of Cr*–pb produces a material that displays the EPR resonance for Cr(III) as well as an isotropic, narrow peak for Cr(V),[19] as seen in Figure 4b. Oxidation of Cr–pb also produces mixed oxidation states of chromium, as seen in Figure 4c; here, however, the signal for Cr(V) is nearly axial due to the presence of g values in both perpendicular and parallel environments. The $g_{\parallel}$ component is observed to contain two distinct values. These latter two signals, at g values of 1.944 and 1.918, may arise from Cr(V) in two different environments produced when sample Cr–pb is oxidized. In contrast, no axial environment is evident for chromium(V) in sample Cr*–pb. We hypothesize that for the latter material Cr(V) is only located at one type of site and that this site is within the hydroxy–aluminum pillar.

B. Decane Cracking. 1. Activity. In Figure 5, conversion of *n*-decane is plotted vs. the number of cycles for each sample. Comparing cracking data for the nonpillared clay (b) and the pillared clay (pb) reveals that the effect of pillaring increases the initial activity of the catalyst but decreases the stability with conversion falling by about 7% in 10 cycles for pb.

Adding Cr(III) ions to a clay, whether pillared or not, results in an increase of the conversion with respect to b and pb, and improves the overall behavior of the catalyst. Cr–b, Cr–pb and Cr*–pb show high initial conversions and improved stability over 10 cycles compared to non-Cr(III)-containing catalysts. Pillaring Cr–b to form Cr–pb maintains high conversion, but both of these catalysts lose a definite d_{001} spacing as shown in the XRD data of Table II. This indicates that chromium ions are of major

(27) Lever, A. B. P. *Inorganic Electronic Spectroscopy*; Elsevier: Amsterdam, 1968.

importance for these catalysts, since the ions are presumed even more accessible when the clay has lost part of its crystalline structure. These samples also show the greatest percentage of Cr, as seen in Table I, which may also be a factor in the high conversions. In long-term experiments carried out to 20 cycles, the pillared clay (Cr-pb) is observed to be less stable.

Among the Cr(III)-containing catalysts, the pillared sample with Cr(III) presumed in the pillar (Cr*-pb) shows 100% conversion over 10 cycles, indicating high activity and high stability.

2. Selectivity. As received Bentolite L (b) is most selective for hexanes formation, as seen in Table V. Pillaring this (pb) produces a lower yield of hexane that decreases with time on stream. Cr*-pb does not produce significant amounts of products heavier than C_5; the major products from this catalyst are light hydrocarbons and coke. It appears, therefore, that a small amount (0.44 wt %) of chromium(III) in the pillars of pillared bentonite creates significant differences in catalytic hydrocracking.

3. Coking. The markedly higher yields of coke for the pillared clays follows a pattern previously reported by Occelli et al.[28] who observed greater yields of coke with PILC's than with H-Y zeolite during gas oil cracking. This was attributed in part to the open, two-dimensional structure of PILC's, which allows easier access for heavier hydrocarbons. Polycondensation reactions and coke formation is typical for Lewis acid sites abundant in PILC's.

During gas-oil conversion[4] typical coking results are 7.8% C (coke/feed) for bentonite and 12.2% C for a pillared bentonite, i.e. approximately 65% higher. These values are in general agreement with our coke yields of 20% C for b and 38% C for pb. Adding Cr(III) ions to a bentonite drastically reduces the amount of coke formation, giving a value of only 4% C over four times as many cycles. Pillaring Cr-b increases the yield of coke to 12% C in 25 cycles. Significantly less coke (22% C) is observed when Cr(III) is added to the pillar (Cr*-pb) with respect to pb; this simultaneously increases the overall conversion as well. This is a further indication of significant catalytic effects associated with the location of Cr(III) ions. Cr-b and Cr-pb display lower coke yields per cycle than pb and Cr*-pb.

The effects of the presence of zirconium(IV) ions in a pillar has also been studied by Occelli et al.[8] By a comparison of APC and (Zr,Al)PC during propylene oligomerization at 480 °C, it was determined that (Zr,Al)PC produced less aromatics and more olefins and aliphatics and displayed less coke formation. APC had 17.2% C on the catalyst while (Zr,Al)PC had only 11.7% C. This was correlated to Lewis acidity. Coke yields for Cr(III)-doped PILC's may, therefore, also be a function of acidity, and we intend to explore this in future experiments.

Further experiments are now in progress to study different catalytic conditions, the role of the metal ion, and the feasibility of extending the use of these catalysts to heavier molecular weight hydrocarbons.[29]

V. Conclusions

Diffuse reflectance and EPR spectroscopies indicate that chromium(III) ions in PILC's can exist in different environments depending on the methods of synthesis; two such important environments appear to be the micropore structure and in the pillar. Heating these catalysts in air converts the chromium to mixed oxidation states (e.g. III, V), but the major contributor appears to remain Cr(III). Catalytic activity for hydrocracking *n*-decane was strongly dependent on the location of the Cr(III) ions. Compared to a clay pillared with pure alumina, a PILC with Cr(III) apparently incorporated into the pillars was more active and more stable as a catalyst for hydrocracking *n*-decane.

Acknowledgment. The National Science Foundation, Grant No. CBT-8317876, supported this work. We thank Dr. Michael Seltzer of the Chemistry Department for suggestions concerning atomic absorption experiments, Southern Clay Products for providing bentonite clays, and Reheis Chemical Co. for providing the Chlorhydrol solution.

Registry No. Cr, 7440-47-3.

(28) Occelli, M. L.; Lester, J. E. *Ind. Eng. Chem. Prod. Res. Dev.* **1985**, *24*, 27.

(29) Skoularikis, N. D.; Carrado, K. A.; Kostapapas, A.; Suib, S. L.; Coughlin, R. W., manuscript in preparation.

Contribution from the Lehrstuhl für Theoretische Chemie, Ruhr-Universität Bochum, D-4630 Bochum, FRG

CEPA Calculations on Open-Shell Molecules. 7. Electronic Structure and Properties of HNS

Jan Wasilewski† and Volker Staemmler*

Received March 5, 1986

The HNS radical has been studied by quantum-chemical ab initio calculations in its lowest electronic states and in two isomeric forms, HNS and NSH. The calculations have been performed at the SCF level and with inclusion of electron correlation effects by means of the CEPA method. Equilibrium geometries, dipole moments, and force fields have been determined for the lowest electronic states as well as excitation energies, dissociation energies, ionization potentials, and electron affinities. HNS has a closed-shell $^1A'$ ground state with R_{NH} = 1.03 Å, R_{NS} = 1.59 Å, and ϑ_{HNS} = 107°. The lowest excited states are only 0.29 ($^3A''$) and 0.96 eV ($^1A''$) above the ground state. NSH has also a $^1A'$ ground state which is 1.02 eV (23.4 kcal/mol) higher than the $^1A'$ ground state of HNS and has an equilibrium geometry with R_{NS} = 1.52 Å, R_{SH} = 1.41 Å, and ϑ_{NSH} = 109°. It seems that the barrier for thermal isomerization between these two isomers is not lower than the lowest dissociation energy (to H + NS). The bonding situation is discussed by using the results of population analyses.

1. Introduction

Sulfur imide (thionitroxyl), HNS, is an unknown molecule that so far has not been observed in isolated form. Only recently it was identified as a bridge ligand in an Fe_2 complex,[1] but its electronic structure in the complex is probably very different from that of isolated HNS. Some thionitroso compounds of the form RNS have been observed as ligands in Fe_2 complexes as well (see ref 1 and references cited therein) or have been proposed as unstable organic compounds.[2]

†Permanent address: Institute of Physics, Nicholas Copernicus University, PL-87100 Torun, Poland.

(1) Herberhold, M.; Bühlmeyer, W. *Angew. Chem.* **1984**, *96*, 64; *Angew. Chem., Int. Ed. Engl.* **1984**, *23*, 80.
(2) Mehlhorn, A.; Sauer, J.; Fabian, J.; Mayer, R. *Phosphorus Sulfur* **1981**, *11*, 325.

0020-1669/86/1325-4221$01.50/0